SKY-GROUND REGION SEGMENTATION AND HORIZON DETECTION USING MULTI-SCALE DARK CHANNEL IMAGES

Meng Ding[1] and Li Wei[2]

[1]College of Civil Aviation
[2]Jincheng College
Nanjing University of Aeronautics and Astronautics
No. 29, Jiangjun Street, Nanjing 211106, P. R. China
nuaa_dm@hotmail.com; nuaa_weili@sina.com

ABSTRACT. *In vision-based navigation and some other function models of many aerial or ground-based robotic systems, sky-ground region segmentation and horizon detection often serve as a preliminary step. This paper proposes an approach of the sky-ground region segmentation and horizon detection using dark multi-scale channel images and their histograms. The approach is divided into three parts. First, multi-scale dark channel images and corresponding histograms are calculated by selecting different sizes of patches. Second, according to the standard deviations of different intervals in multi-scale histograms, each histogram of multi-scale dark channel images can be divided into five intervals including darkest, dark, middle, light and lightest interval. The threshold value for sky-ground region segmentation is obtained by selecting the gray value corresponding to the minimum value of the vertical axis in the middle interval of the histogram. Third, the dark channel image with larger size patch is used for sky region determination by picking its top brightest pixels. Experimental results show this approach based on dark channel instead of the blue color component and minimum value of the middle interval of dark channel histogram instead of Otsu's method can finish sky-ground region segmentation and horizon detection better.*
Keywords: Sky-ground region segmentation, Horizon detection, Multi-scale dark channel image

1. **Introduction.** Sky-ground region segmentation and horizon detection play an important role in vision-based navigation and some other function models of various aerial or ground-based robotic systems [1-3]. The purpose of sky-ground region segmentation and horizon detection is to search a line or curve with the highest likelihood of separating sky region from ground region in a given image. For the ground-based mobile robots, sky-ground region segmentation and horizon detection may be the preliminary step of path searching and road searching [4]. For unmanned aerial vehicles (UAV), it is the first problem of automatic safe landing-site search system to identify where the ground is and detect horizon when the sky and ground regions both appear in the image [5]. For micro air vehicles (MAV), the roll angle which is an essential parameter for MAV control system can be calculated directly based on the result of horizon detection [1,6]. Therefore, it is very necessary to study autonomous horizon detection.

As you know, identifying the horizon between ground and sky region is very straightforward for humans. Nevertheless, there are also some significant challenges in autonomous horizon detection. Within the last two decades, several approaches of horizon detection have been proposed [7-11]. Since the scene of the ground and sky in given images varies dramatically based on the time of day, the current weather and the specific terrain, all of these approaches are established on restrictive assumptions which include: Firstly, the pixel characteristics of the sky region are thought to be consistent and have little

variance which can be estimated by the mean and standard deviation of image patches. Secondly, the horizon is assumed to be a straight line and the strongest boundary which can be detected by using Hough transform from the edge map is obtained by edge detector [12]. Thirdly, the bottom of the image acquired by a camera which is mounted on a ground-based robot can be set as the ground region. The above assumptions limit the scope of these methods' application and cause several problems. For example, due to the first assumption, the algorithm of horizon detection may fail when the large objects have similar pixel characteristics to the sky region (i.e., lakes, rivers, roads). For the second assumption, sometimes the horizon in the image is not a straight line or the strongest edge on account of the artificial buildings or mountains on the ground. Moreover, the third assumption is not suitable for the images captured by the camera fixed on UAV or MAV.

This paper proposes an autonomous horizon detection algorithm using dark channel image [13-15]. Conception of dark channel comes from an observation on outdoor images. Related statistics indicates that in most of the local regions which do not cover the sky region, at least one color (RGB) channel (called dark channel) has some pixels whose intensities are very low and close to zero [13]. According to this observation, we can obtain a fact that the intensities of the ground region are significantly less than the intensities of the sky region in the dark channel image. Because of the difference of the pixel distribution between sky and ground region in the dark channel image, a reliable algorithm of sky-ground region segmentation and horizon detection is proposed.

The remainder of this paper is organized as follows. The proposed method for autonomous horizon detection is explained in Section 2. The experimental results are given in Section 3, and conclusions are presented in Section 4.

2. Method.

2.1. Multi-scale dark channel images computation.
In digital image processing, a color image has three channels: Red(R), Green(G), and Blue(B). In other words, the color image is composed of three matrixes (one for each channel), where each image can store discrete pixels with conventional brightness intensities between 0 and 255. In accordance with this structure, the conception of the dark channel is defined as follows: For an arbitrary original image $\mathbf{A}$, its dark channel $\mathbf{A}^{\mathrm{dark}}$ is given by:

$$\mathbf{A}^{\mathrm{dark}}(x_0, y_0) = \min_{\substack{x \in \{x_0-n,\cdots,x_0,\cdots,x_0+n\} \\ y \in \{y_0-n,\cdots,y_0,\cdots,y_0+n\}}} \left(\min_{C \in \{R,G,B\}} \mathbf{A}^{\mathrm{C}}(x, y) \right) \tag{1}$$

where $\mathbf{A}^{\mathrm{C}}$ is a color channel of $\mathbf{A}$ and includes $\mathbf{A}^{\mathrm{R}}$, $\mathbf{A}^{\mathrm{G}}$ and $\mathbf{A}^{\mathrm{B}}$ corresponding to red, green and blue channel respectively, the size of the local patch centered at (x_0, y_0) is $(2n+1) \times (2n+1)$, multiscale dark channel images can be obtained by selecting different n. $\mathbf{min}(.)$ is a minimum filter and two $\mathbf{min}(.)$ are commutative. In the practical application, $\mathbf{min}(.)$ is computed by Van Herk's fast algorithm which has been used in reference [13]. Conception of dark channel means that if $\mathbf{A}$ is an outdoor clear image, except for the sky region, the intensity of $\mathbf{A}$'s dark channel is low and near to zero.

Figure 1(a) is an image captured by a camera mounted on a fixed-wing UAV. Figures 1(b), 1(c), 1(d), 1(e) are its dark channel images using 3×3 ($n = 1$), 21×21 ($n = 10$), 41×41 ($n = 20$), 61×61 ($n = 30$) respectively. In these dark channel images, we can find that the intensities of the sky region are larger than that of no-sky region obviously. Generally, there are three main factors which induce the low intensity in the dark channel including shadows of the landscape images, colorful objects or surfaces with low reflectance in any channel which will result in low values in the dark channel (e.g., green grass and yellow land in Figure 1(a)), and dark objects or surfaces.

FIGURE 1. Sample image and its multi-scale dark channel images using different size patches

In Equation (1), the patch size is a key and unique varying parameter in dark channel algorithm. From Figure 1, we can conclude that the larger the patch size is, the darker the dark channel is. In other words, the performance of the dark channel image becomes better for a larger patch size since the probability that a patch covers a pixel with the lower intensity is increased. For sky-ground region segmentation and horizon detection, because the scope of the sky region is constant, the high intensity interval (from 150 to 255) of the histogram representing the sky region remains stable.

2.2. **Threshold segmentation.** As previously mentioned, the intensities of the sky region are higher than of no-sky region obviously in dark channel image. Therefore, the sky region can be extracted from dark channel image by selecting a threshold T. Just because of this, the threshold value selection becomes important for the sky-ground region segmentation. In image processing and computer vision, the most usual approach for automatic threshold selection is Otsu's method. This paper proposes a new approach of threshold selection based on the normalized histograms of multi-scale dark channel images. Considering the intervals of the histogram denoting sky region are invariable as the size of patch changes, the histogram is divided into five parts according to the interval of the horizontal axis: darkest interval (P_1), dark interval (P_2), middle interval (P_3), light interval (P_4), lightest interval (P_5):

$$P_1 = \sum_{i=0}^{50} p_i, \quad P_2 = \sum_{i=51}^{100} p_i, \quad P_3 = \sum_{i=101}^{150} p_i, \quad P_4 = \sum_{i=151}^{200} p_i, \quad P_5 = \sum_{i=201}^{250} p_i \qquad (2)$$

For the dark channel images of Figure 1, the values of P_1-P_5 corresponding to different size patches ($n = 1$ to 30) are shown in Figure 2. Figure 2 reveals that the values of P_1 monotonically and significantly increase, P_2 dropped dramatically, P_3 slowly declined, and P_4 and P_5 are relatively stable as the patch size grows. This variation tendency of Figure 1 indeed follows the rule that the larger the patch size is, the darker the dark channel is. According to this rule, the horizontal axis scope of the histogram corresponding to P_4 and P_5 can represent the intensities of the sky region. We select a threshold value T which corresponds to minimal value of the vertical axis between 101 and 150 of horizontal axis (middle interval) of the histogram. Figure 3(a) shows that the intensity value corresponding to minimal value of the vertical axis of the histograms is stable as the patch size increases. Therefore, T = 138 and the result of image segmentation which has been further processed by morphology method is shown in Figure 3(b). The white region of Figure 3(b) can be divided into five independent parts and the largest one is in the upper half of the image.

2.3. **Sky region determination.** In general, the region containing the brightest pixels of the original image is considered to the sky region. This is correct only when the weather is overcast and the sunlight can be ignored [13]. Unfortunately, the sunlight can be rarely ignored in practice. For instance, the brightest pixels of an original image may be on a white car or a white building. As discussed in Section 2.2, the intensity scope of sky region is higher than no-sky region in dark channel image. Therefore, we can determine sky region by picking the top 0.1% brightest pixels in the dark channel image. Note that the brightest pixels in the dark channel image may not be the brightest ones in the original
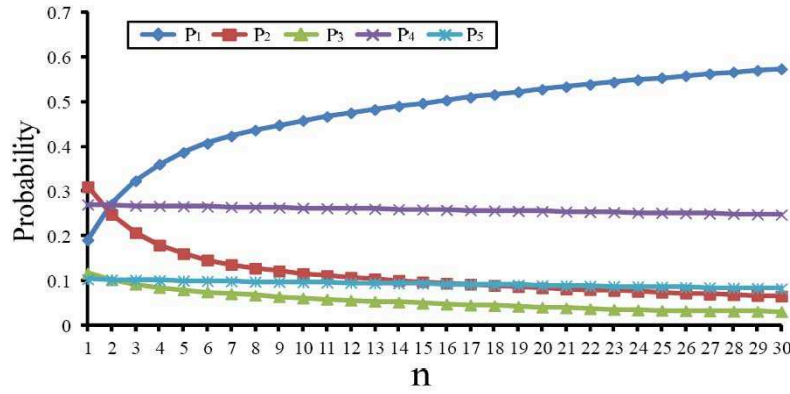
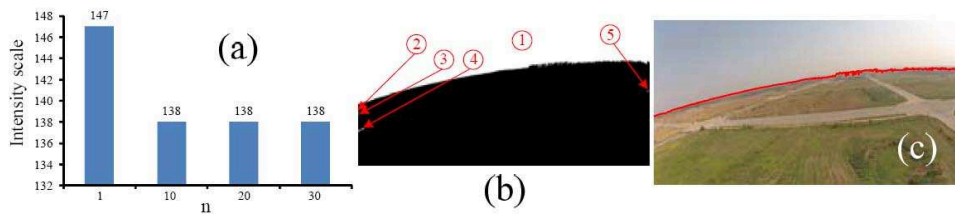FIGURE 2. Variation of P_1-P_5 corresponding to different size patches ($n = 1$ to 30)

FIGURE 3. (a) T according to different n; (b) image segmentation with T = 138; (c) detected horizon
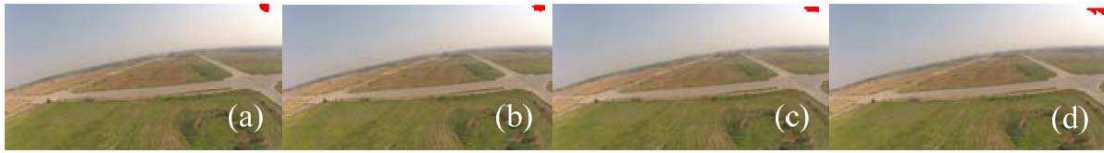

FIGURE 4. The brightest pixels in the dark channel images with different n: (a) $n = 1$; (b) $n = 10$; (c) $n = 20$; (d) $n = 30$

image. Figure 4 shows the brightest pixels in the dark channel images with different size patches. Although the brightest pixels are not identical in different dark channel images, the positions of these pixels correspond to the largest white sub-region (No. 1 of Figure 3(b)). Therefore, this sub-region can be determined as the sky region and the horizon also can be obtained using the edge of the sky region (Figure 3(c)).

3. **Experimental Results and Discussion.** In this section, we first present experiments on six images captured by a camera mounted on a fixed-wing UAV for sky-ground region segmentation and horizon detection to demonstrate the efficacy of the proposed algorithm. Second, we compare our approach with Cheng's work [11]. Lastly, the relationship between the brightest pixels in the dark channel image and the patch size of the dark channel is discussed which is important to sky region determination.

3.1. **Sky-ground region segmentation and horizon detection.** According to the method described in Section 2, threshold values of six images are calculated and the corresponding results of horizon detection are shown in Figure 5. The final results of horizon detection show the effectiveness of the proposed approach.

3.2. **Comparison with Cheng's work.** In general, horizon detection can be divided into region-based and edge-based method. The proposed method belongs to the first one. As a representative region-based method, Cheng's method selected blue color component
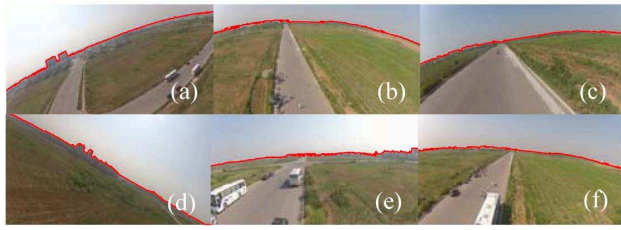
FIGURE 5. Horizon detection: (a) T = 143; (b) T = 141; (c) T = 123; (d) T = 142; (e) T = 148; (f) T = 139
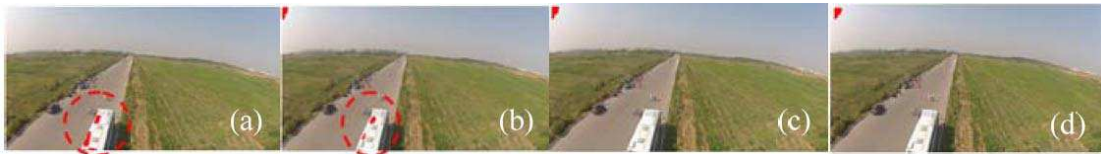
FIGURE 6. Result using Cheng's method

FIGURE 7. The brightest pixels of Figure 5(e): (a) $n = 1$; (b) $n = 10$; (c) $n = 20$; (d) $n = 30$

FIGURE 8. The brightest pixels of Figure 5(f): (a) $n = 1$; (b) $n = 10$; (c) $n = 20$; (d) $n = 30$

of original image and used Otsu's method to obtain segmentation threshold [11], and the segmented image and the boundary of sky and ground region are shown in Figure 6. By comparing our approach (the result shown in Figure 3(c)) with Cheng's work, we find that the approach based on dark channel can finish horizon detection better.

3.3. **Relationship between position of the brightest pixels and patch size of dark channel.** Our approach determines sky region by picking the top 0.1% brightest pixels in the dark channel image. Red points of Figure 7 and Figure 8 correspond to the top 0.1% brightest pixels in different dark channel images using 3×3, 21×21, 41×41 and 61×61 patches. Because there is a white bus in the image, some of the brightest pixels are on bus region (red circle) in Figures 7(a), 7(b) and Figure 8(a). Meanwhile, we can find that when using larger size patches (shown in Figures 7(c), 7(d) and Figures 8(b), 8(c), 8(d)), this error can be avoided. Therefore, we need to use dark channel image with larger size patch to pick the top brightest pixels in the process of sky region determination. However, this approach also has its own limitation. For example, when the color of the scene object is white or nearly white and the size of this scene is big enough, the method to search the brightest pixels in dark channel image may be invalid.

4. **Conclusions.** This paper proposed an algorithm of the sky-ground region segmentation and horizon detection. The paper suggests three conclusions: (1) Multi-scale dark channel images can be used for sky-ground region segmentation and horizon detection according to the statistics characteristic that the larger the patch size is, the darker the dark channel is. (2) An efficient threshold value can be obtained by selecting minimum value of the vertical axis in the middle interval of the histogram. (3) In the process of sky

region determination, in order to avoid interference of white objects in the original image, we need to use a dark channel image with larger size patch to pick the top brightest pixels.

REFERENCES

[1] M. S. Ettinger, C. M. Nechyba, G. P. Ifju and M. Waszak, Vision-guided flight stability and control for micro air vehicles, *Proc. of IEEE/RSJ International Conference on Intelligent Robots and System*, Lausanne, Switzerland, vol.3, pp.2134-2140, 2002.

[2] G. Bao, S. Xiong and Z. Zhou, Vision-based horizon extraction for micro air vehicle flight control, *IEEE Trans. Instrumentation and Measurement*, vol.54, no.3, pp.1067-1072, 2005.

[3] Y. Kim and H. Kim, Layered ground floor detection for vision-based mobile robot navigation, *Proc. of IEEE International Conference on Robotics and Automation*, New Orleans, USA, vol.1, pp.13-18, 2004.

[4] S. Williams and A. Howard, Horizon line estimation in glacial environments using multiple visual cues, *Proc. of IEEE International Conference on Robotics and Automation*, Shanghai, China, pp.5887-5892, 2011.

[5] Y. F. Shen, Z. Rahman, D. D. Krusienski and J. Li, A vision-based automatic safe landing-site detection system, *IEEE Trans. Aerospace and Electronic Systems*, vol.49, no.1, pp.294-310, 2013.

[6] W. J. Xu, P. Li and B. Han, Horizon detection algorithm in extended Kalman filter framework, *Control Theory & Applications*, vol.29, no.2, pp.225-228, 2012.

[7] Y. F. Shen, D. Krusienski, J. Li and Z. Rahman, A hierarchical horizon detection algorithm, *IEEE Geoscience and Remote Sensing Letters*, vol.10, no.1, pp.111-114, 2013.

[8] D. Dusha, W. Boles and R. Walker, Attitude estimation for a fixedwing aircraft using horizon detection and optical flow, *Proc. of Biennial Conference of the Australian Pattern Recognition Society on Digital Image Computing Techniques and Applications*, Glenelg, Australia, pp.485-492, 2007.

[9] S. F. Zhao, H. Zhang and Y. Z. Fan, Attitude estimation method for flight vehicles based on computer vision, *Journal of Beijing University of Aeronautics and Astronautics (Nature Science)*, vol.32, no.8, pp.885-888, 2006.

[10] D. T. Cornall and K. G. Egan, Measuring horizon angle from video on a small unmanned air vehicle, *Proc. of International Conference on Autonomous Robots and Agents*, Palmerston North, New Zealand, pp.339-344, 2004.

[11] X. Cheng, Q. Hao, Y. Song, Y. Hu and K. Zhang, A horizon detection algorithm based on between-class variance analysis, *ACTA AERONAUTICA ET ASTRONAUT ICA SINICA*, vol.31, no.10, pp.2056-2061, 2010.

[12] R. O. Duda and P. E. Hart, Use of the Hough transformation to detect lines and curves in pictures, *Communications of the ACM*, vol.15, no.1, pp.11-15, 1972.

[13] K. M. He, J. Sun and X. O. Tang, Single image haze removal using dark channel prior, *IEEE Trans. Pattern Analysis and Machine Intelligence*, vol.33, no.12, pp.2341-2353, 2011.

[14] M. Ding and R. F. Tong, Efficient dark channel based image dehazing using quadtrees, *Science China (Information Sciences)*, vol.56, no.9, pp.1-9, 2013.

[15] A. K. Tripathi and S. Mukhopadhyay, Single image fog removal using anisotropic diffusion, *IET Image Process*, vol.6, no.7, pp.966-975, 2012.